The Journal of Chemical Physics

The role of thermal history on spontaneous polarization and phase transitions of amorphous solid water films studied by contact potential difference measurements

Cite as: J. Chem. Phys. **153**, 144702 (2020); https://doi.org/10.1063/5.0017712
Submitted: 09 June 2020 • Accepted: 21 September 2020 • Published Online: 08 October 2020

Roey Sagi, Michelle Akerman, Sujith Ramakrishnan, et al.

The Journal of Chemical Physics ARTICLE scitation.org/journal/jcp

The role of thermal history on spontaneous polarization and phase transitions of amorphous solid water films studied by contact potential difference measurements

Cite as: J. Chem. Phys. 153, 144702 (2020); doi: 10.1063/5.0017712
Submitted: 9 June 2020 • Accepted: 21 September 2020 •
Published Online: 8 October 2020

Roey Sagi, Michelle Akerman, Sujith Ramakrishnan, and Micha Asscher[a)]

AFFILIATIONS

Institute of Chemistry, The Hebrew University of Jerusalem, Edmond J. Safra Campus, Givat-Ram, Jerusalem 9190401, Israel

[a)]Author to whom correspondence should be addressed: micha.asscher@mail.huji.ac.il

ABSTRACT

Monitoring thermal processes occurring in molecular films on surfaces can provide insights into physical events such as morphology changes and phase transitions. Here, we demonstrate that temperature-programmed contact potential difference (TP-ΔCPD) measurements employed by a Kelvin probe under ultrahigh vacuum conditions and their temperature derivative can track films' restructure and crystallization occurring in amorphous solid water (ASW) at temperatures well below the onset of film desorption. The effects of growth temperature and films' thickness on the spontaneous polarization that develops within ASW films grown at 33 K–120 K on top of a Ru(0001) substrate are reported. Electric fields of ~10^6 V/m are developed within the ASW films despite low average levels of molecular dipole alignment (<0.01%) normal to the substrate plane. Upon annealing, an irreversible morphology-dependent depolarization has been recorded, indicating that the ASW films keep a "memory" of their thermal history. We demonstrate that TP-ΔCPD measurements can track the collapse of the porous structure at temperatures above the growth and the ASW-ice I_c and ASW-ice I_h transitions at 131 K and 157 K, respectively. These observations have interesting implications for physical and chemical processes that take place at the interstellar medium such as planetary formation and photon- and electron-induced synthesis of new molecules.

I. INTRODUCTION

Water-ice covered grain mantles are abundant in the universe, since water is the most abundant molecular ice constituent in the interstellar medium (ISM) and in molecular clouds (MC).[1] Condensation of gas-phase molecules on grains forms pure or mixed icy layers due to the low temperature typical to these environments (10 K–100 K), growing amorphous films such as the amorphous solid water (ASW). These ices are important in physical and chemical processes that occur in these environments. For example, they host photo- and radiation-induced chemical reactions and are presumed to affect gravitational collapse and agglomeration of dust grains at the early stages of stellar system formation, specifically in the case of polar films.[2–4] With its gas-phase dipole moment of 1.85 D, water has the potential to form polar solid films. This possibility has drawn considerable attention throughout the past few decades. Crystalline water, both the hexagonal ice (ice I_h) and the cubic ice (ice I_c), should not exhibit any spontaneous polarization (though the hydrogen-ordered phase, ice XI, does),[5] since every dipole is balanced by its neighbors. Nonetheless, it is possible to form polar ASW films.

At the limit of a very low sub-monolayer coverage, the dipole moment of a surface-adsorbed water molecule is isolated of any dipole–dipole interactions with its nearest neighbors; thus, it is adsorbate-density independent. It is only affected by its interaction with the substrate, due to the possible charge transfer to the support, and the interaction with the image dipoles within it (considering a conducting substrate). In the case of denser films, dipole–dipole

interactions must be taken into account. When the dipoles continue to accumulate and the polarized film becomes thicker, the voltage difference between the two "electrodes" (film's top and bottom) is affected too. Ideally, lateral random internal dipole-orientations should cancel each other, leaving only the dipoles at the interfaces. This leads to the formation of an internal electric field, which further directs the dipoles. However, this positive feedback inside the ice matrix is limited due to the frustrated mobility imposed on an individual dipole by those surrounding it and the low growth temperature.

The films' polarization can be determined by the voltage developed between the two electrodes. A standard and simplistic view of the voltage developed can be expressed as[6]

$$\Delta V = \frac{M_{(T)}\tilde{\mu}_{z(T)}}{A\varepsilon_0\varepsilon_{(T)}}, \tag{1}$$

where M is an integer representing the effective number of dipoles with some "up" orientation tendency (the difference between the total number of dipoles with "up" orientations and those with "down" orientations, $N_\uparrow - N_\downarrow$). $\tilde{\mu}_z$ is the z-axis component (normal to the substrate surface) of the averaged molecular dipole moment, which indicates the overall degree of polarization of the film, A is the substrate area, ε_0 is the vacuum permittivity ($\simeq$8.85 $\times$ 10^{-12} C V^{-1} m^{-1} or for convenience 2.66 $\times$ 10^{14} D V^{-1} cm^{-2}, where 1 D = 3.33 $\times$ 10^{-30} C m), and $\varepsilon_{(T)}$ is the relative permittivity of the film, often taken as 3.2 for solid water below 150 K.[7,8] The electric field should not contain any lateral contributions, only the z-component (E_z), and can be calculated according to

$$E_z = \frac{d(\Delta V)}{dz}. \tag{2}$$

By having the internal electric field and by the mean-field approach, one can calculate the aligned molecular dipole moment, which is as follows:[9]

$$\tilde{\mu}_z = \varepsilon_0\Omega\frac{d(\Delta V)}{dz}, \tag{3}$$

where Ω is the molecular volume.

One possible way to measure the voltage difference across a film is by contact potential difference (CPD) measurements, monitoring the surface work function change upon film growth, relative to that of the clean substrate. This is plausible because adsorption, and particularly chemisorption on metal surfaces, alters the surface charge distribution. Such measurements of the spontaneous evolution of a voltage difference, ΔCPD, during the growth of thick ASW films by condensation of water vapors on metal surfaces were previously reported, mostly on Pt(111),[7,10] Ru(0001),[11–13] and gold coated quartz microbalance.[14–16] These studies have introduced the pyroelectric nature of water films[7,10] and the influence of film morphology, mostly the porosity, on the potential difference.[14–16] Measurements on the Ru(0001) surface (employing ΔCPD) included the growth of the first monolayers (MLs)[11,12] of water and a recent report from our group concerning the temperature-dependent charging of thick ASW films by low-energy electrons.[13] All these reports focused on the growth conditions, especially growth temperatures, either to distinguish between the amorphous and crystalline phases or to emphasize the role of morphology. It is well established that the morphology of ASW films is strongly affected by the growth temperature;[17–21] the film becomes more porous at low growth temperatures (other factors contributing to the ASW film porosity are the vapor flux during growth, i.e., the growth rate,[21] and the incidence angle in the case of molecular beam depositions[22]). The measurements discussed below are of interest because they can further illuminate the macroscopic dielectric properties of the icy film and how it is influenced by the substrate temperature and structure during its growth. Moreover, the *in situ* nature of the ΔCPD measurements enables detection of polarization-changes the films undergo upon temperature modifications (e.g., programmed annealing).

Temperature-programmed ΔCPD (ΔΦ-TPD or TP-ΔCPD) measurements, and more specifically their temperature derivative [d(ΔCPD)/dT], can be compared to the standard temperature-programmed desorption (ΔP-TPD) measurements[23] as both show similar profiles. The standard ΔP-TPD measurements provide information on the binding energies of adsorbates to the substrate (in the sub-monolayer regime) and the intermolecular interactions.[11,12,24–27] ΔCPD measurements provide additional information on the macroscopic molecular orientation and its response to film heating and can potentially track morphological changes together with phase transitions that take place while the film temperature varies, prior to any desorption. Performing ΔCPD measurements to monitor such structural modifications via polarization changes is the focus of this report.

II. EXPERIMENTAL METHODS

Hundreds of monolayer (ML)-thick ASW films were grown on a Ru(0001) substrate (8 × 8 × 2 mm^3) attached to a closed-cycle He refrigerator (Janis) under ultrahigh vacuum (UHV) conditions (base pressure of <2 × 10^{-10} Torr). The cryostat cools the sample down to a temperature of 33 K. We could accurately set the sample's temperature by utilizing a Si diode and a 50 Ω cartridge heater, attached to the bottom of the cryostat and controlled by a LakeShore 335 temperature controller. This configuration enables temperature control in the range of 33 K–300 K. In addition to the silicon diode sensor, the temperature readings of the ruthenium sample at higher temperatures at higher temperatures were obtained by a K-type thermocouple spot-welded at the side of the substrate, providing an accuracy of ±0.5 K. Substrate heating is performed by a resistive heating of two 0.4 mm diameter Ta wires spot-welded to the top and bottom edges of the Ru(0001) crystal. A LabVIEW algorithm enables both monitoring the temperature and controlled heating/cooling of the sample at constant rates in the range of 0.5 K/s–10 K/s. The ruthenium surface is daily sputter-cleaned by 800 eV Ne^+ ions for 12 min, followed by annealing to 1450 K for 3 min. The chamber is equipped with a quadrupole mass spectrometer (QMS, RGA-300, Stanford Research Systems) and a Kelvin probe (KP-S, Besocke-Delta-Phi), which allows ΔCPD measurements. The controlled heating enables ΔP-TPD measurements and to continuously monitor the surface work function changes (ΔCPD) while rearrangements of the adsorbates take place (TP-ΔCPD measurements). This, together with the temperature derivative [d(ΔCPD)/dT] spectra, often provides a unique information on the polarized (or charged) films.[11,23,28–31] The

UHV chamber is further equipped with an electron source (1 eV–2000 eV; ELG-2, Kimball Physics) and a mini-Auger analyzer (LK technologies) for determining the surface cleanliness. Water vapors (H_2O, triple distilled, kept in a glass ampule that was further purified by several freeze–pump–thaw cycles) were introduced by backfilling the UHV chamber through a high-precision leak valve, ensuring homogeneous coverage on the sample and its cold surroundings. The exposure of a 1 ML (calculated in Langmuir units, L, where 1 L = 10^{-6} Torr s) thick film was derived from the onset of the water multilayer desorption peak (near 155 K) while performing exposure-dependent ΔP-TPD measurements. A 1 ML of H_2O is equivalent to the exposure of 1.0 ± 0.1 L under our specific experimental setup.

III. RESULTS AND DISCUSSION

A. ASW film polarization

Deposition of water molecules on the Ru(0001) substrate was performed at a substrate temperature in the range of 33 K–120 K at a fixed growth rate of 1 ML/s while continuously recording the ΔCPD. In Fig. 1(a), the ΔCPD profiles measured during the film growth, up to 700 ML-thick films at different growth temperatures (denoted by T_{gr}), are shown. When exposure approached the desired value, vapor pressure was sharply reduced, and at sufficiently low pressures, the substrate was cooled down to 33 K.

The ΔCPD profiles during growth demonstrate a strong substrate temperature dependence, revealing a complex behavior, at

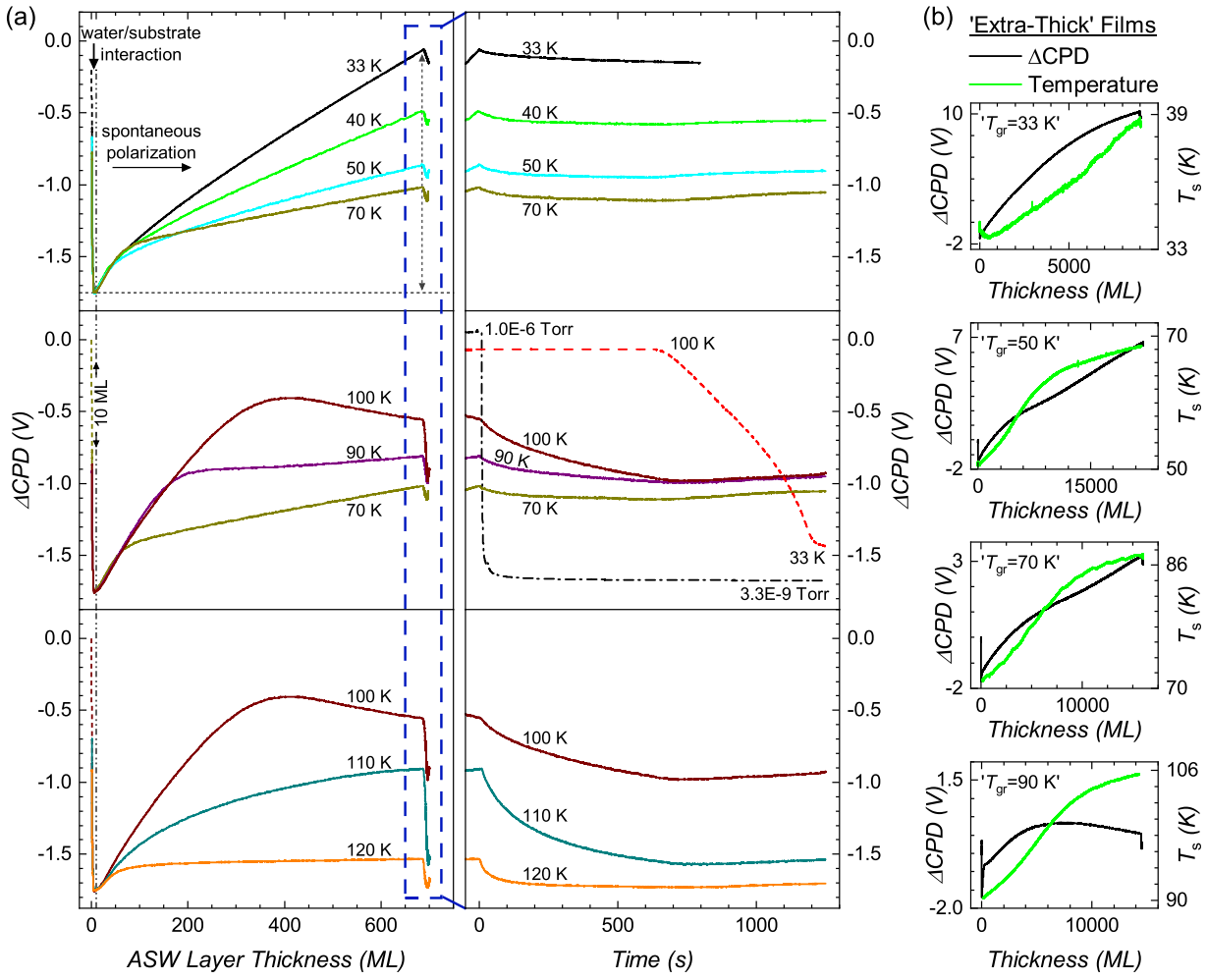

FIG. 1. Contact potential difference change (ΔCPD) curves during the growth of ASW films on top of a Ru(0001) substrate at the temperature range of 33 K–120 K (denoted by T_{gr}) at a fixed growth rate of 1 ML/s. (a) Growth of 700 monolayer (ML)-thick films (in the left-hand side panels); the blue (vertical) dashed rectangle (centered at 700 ML) denotes exposure termination (leak-valve closure; initiates the observed voltage-drop). Films were then cooled down to 33 K. The right-hand side panels of (a) show the ΔCPD vs time curves following the leak-valve closure. A typical pressure-drop profile and a representative substrate temperature profile of a film grown at 100 K and then cooled down to 33 K are demonstrated in the middle-right panel by the black dashed-dotted and red dashed lines, respectively. (b) ΔCPD measurements during the growth of "extra-thick" ASW films (up to 22 000 ML; in black) at the indicated initial growth temperatures and the corresponding during-the-growth substrate temperature profiles (denoted by T_s; in green).

three characteristic growth temperature regions: below 70 K, 70 K–100 K, and above 100 K. For all temperatures, an initial sharp drop of the ΔCPD signal is observed from zero down to a minimum value of −1.75 V, reached at a thickness of ~10 ML [see the left-hand side panels of Fig. 1(a)]. Investigation of the first monolayers of water adsorbed on Ru(0001) by utilizing the work function change (ΔCPD) and ΔP-TPD measurements was reported by Lilach *et al.*[11] These direct measurements of the ΔCPD during film growth showed an initial increase in the dipole moment from the gas-phase value of 1.85 D to 2.2 D when noninteracting dipoles adsorb. This increase in the dipole moment indicates that a partial charge transfer from the oxygen lone pairs to the substrate takes place, since the water molecule chemisorbs through its oxygen. For denser sub-monolayer films, dipole–dipole interactions and hydrogen-bonding need to be considered. At this limit, water molecules form almost planar rings,[32] commensurate with the hexagonal 0001 plane of the substrate. Furthermore, water molecules initially tend to cluster on the Ru surface,[18,32,33] rather than to form a wetting layer. Therefore, an equivalent thickness of several water layers is necessary to completely cover the Ru surface (even up to 100 ML[33]). Those upper-layer molecules still contribute to the measured work function change, however, with gradually smaller influence. Therefore, the T_{gr}-independent minimum ΔCPD value of −1.75 V measured at the ASW layer thickness of 10 ML may indicate the limit of the interaction range of the stacked water layers with the substrate. At thicker films, this stops playing a role, and the substrate becomes irrelevant for the determination of ΔCPD from that point on. Only interactions between the new-coming dipoles and the already formed macroscopic surface dipole should be considered at the gradually thicker films, resulting in temperature-dependent ΔCPD profiles. Beyond adsorption of 10 ML, the water molecules change their net polarization (rapidly at first and then more moderately), rather than sustaining a random orientation as one would expect from amorphous materials. Up to a thickness of 45 ML, the voltage nonlinearly increases, independent of T_{gr} up to 70 K. Then, the profile breaks with a strong substrate temperature dependence. This break is followed by a linear voltage increase; however, the slope gradually decreases with T_{gr}. In the T_{gr} range of 70 K–100 K, the increase from the minimum obtained at 10 ML is identical to that described before; however, the break previously seen at 45 ML occurs at increasing thicknesses. At T_{gr} = 100 K, a maximum value of ΔCPD is observed at 400 ML, and then, the voltage linearly drops. Above 100 K, the deviation from the initial (positive) slope beyond 10 ML occurs gradually at lower thicknesses. At T_{gr} = 120 K, the voltage saturates early, and no further change in ΔCPD (polarization) evolves. There, the expected random dipole orientation is met.

Porosity, as demonstrated by Bu *et al.*,[14] is a major contributor for the voltage development across ASW films. Water molecules in ASW are distinguished by their infrared absorption band at wavelengths near 3700 cm^{-1}, attributed to O–H stretch vibrations of dangling bonds. Two- and three-coordinated water molecules, which are assigned to the 3720 cm^{-1} and 3696 cm^{-1} features, respectively,[34] populate sites of broken symmetry, e.g., water/vacuum interfaces and structural hydrogen-bond defects. These peaks, therefore, are considered as markers for the water film degree of porosity.[14] For example, compact water layers contain only a small population of low-coordinated (three and two) molecules, while for films grown at low T_{gr} (thus more porous), these peaks are typically strong due to the increased surface area the pores impose. Bu *et al.*[14] showed (based on IR analysis) a nice correlation between the measured voltage across a film and the level of porosity, governed by the growth temperature [note the opposite sign of the voltage in the current work with respect to theirs and of others; the difference stems from our choice to use the substrate/ice interface perspective and not that of the ice/vacuum[13,35] (see Sec. II of the supplementary material)]. In the case of homogeneous porosity across the film, the surface area should linearly increase with the film thickness, and therefore, a linear increase in the polarization is expected.

The break in the slope of ΔCPD vs thickness observed at 45 ML for films grown at temperatures up to 70 K and at gradually increasing thicknesses above 70 K indicates that another change in the structure of the adsorbed water molecules takes place, which results in a lower fraction of alignment of the water molecules with respect to the substrate normal and may arise from morphology. It may also be the result of morphology change the film undergoes. Bu *et al.* also reported that cracking of ASW films occurs above a critical thickness, correlated with the degree of porosity.[15,16] This cracking stems from the porous film tendency to contract in order to reduce the film's free energy, whereas the rigidity of the substrate restricts this propensity. This, in turn, leads to higher stress within the film. Eventually, this is seen as a nonlinear correlation between the developed voltage across the film and the film thickness, which can explain the appearance of this break at increasing thicknesses above 70 K. Another explanation may arise from the island growth mechanism of the first layers, leaving some unexposed patches of the bare metal. It was reported that the island structure holds for high coverages, even up to 100 ML, before the surface is fully covered.[33]

A similar deviation from linearity is observed upon the growth of much thicker films, although originating from a different source. ASW is a poor heat conductor.[36] Under the experimental conditions, the substrate cannot effectively dissipate the excess heat exchange introduced during the condensation of room temperature water vapor onto very thick ASW films (thousands of monolayers; "extra-thick" films).[37] During the growth of 700 ML-thick films, the temperature only mildly increases by ~1 K [see Figs. S1(a)–S1(f) of the supplementary material]. However, for much thicker films, up to 22 000 ML (growth rate of 1 ML/s as for the 700 ML-thick films), it increases significantly more, up to 20 K [Fig. 1(b), and Figs. S1(g)–S1(j) of the supplementary material; except for the films grown at initial T_{gr} of 33 K, for which the substrate cooling is more effective due to the heat conductivity characteristics of a sapphire disk separating the cryostat from the sample holder]. This can be exploited to further demonstrate the temperature effect on the ΔCPD evolution during the growth. These extra-thick films were grown at initial temperatures in the range of 33 K–90 K and exhibit nonlinear ΔCPD vs thickness profiles. As discussed previously, above the thickness of 45 ML, the ΔCPD profile is linear; however, in the thickness range of 1000 ML–7600 ML, the ΔCPD increases but at a decreasing slope (thus is concave). At the thickness of 7600 ML, one can observe an inflection point that leads to a further linear ΔCPD increase [Fig. 1(b), and Figs. S1 and S2 of the supplementary material]. Exceptions are the films that were grown at 33 K and 90 K. For the former, linearity beyond 10 V is only assumed, since the ΔCPD approaches an instrumental limitation of 10 V before any linear voltage increment can be observed.

The latter reveals a ΔCPD maximum (at 7600 ML) before it decreases. The ΔCPD concavity is accompanied by a convex substrate temperature profile [T_s in Fig. 1(b); rises gradually with increasing rates]. These trends switch around the ΔCPD inflection point; while the rate of temperature-increase drops, the ΔCPD profile regains its linearity with the thickness [see Fig. S2(b) of the supplementary material]. We conclude that a counter-correlation between the temperature behavior and that of the ΔCPD measurements is observed as a function of thickness. The quantitative explanation of the temperature increase during growth is not well understood at this point and requires, therefore, further studies.

Temperature increase during the growth process decreases somewhat the porosity of the film,[21] in this case mostly at the upper portion of the film that approaches the ASW/vacuum interface, forming a vertical porosity gradient. The gradual decrease in porosity away from the substrate lowers the level of polarization at these upper layers.[14] A stable film temperature during growth results in a homogeneous porosity within the entire film; hence, a linear ΔCPD profile is expected [with either a positive or negative slope; Figs. S1(a)–S1(f) of the supplementary material]. This discussion also shows that the deviation from linearity of the ΔCPD vs thickness profiles between the minimum ΔCPD value of −1.75 V at 10 ML and the break in the ΔCPD slope at 45 ML for T_{gr} up to 70 K originates from a different source. This is apparent because only a mild temperature change is experienced during this stage of growth [Figs. S1(e) and S1(f) of the supplementary material].

Films of intermediate thickness grown at 100 K and extra-thick films grown at 90 K reveal another similarity. For both, a net orientation (polarization) flipping (a change in the sign of the slope of ΔCPD vs film thickness) following the discussed maximum is observed. For the extra-thick films grown at 90 K, the ΔCPD profile exhibits a maximum at 7600 ML, a thickness in which the temperature was ramped from 90 K to ~100 K. It points out for a possible mechanism for polarization flipping, with the T_{gr} threshold of ~100 K.

Growth termination occurs when the leak valve is closed and the vapor pressure drops. This event results in a reduction of the ΔCPD (seen inside the blue dashed rectangle in the left-hand side panels of Fig. 1(a) following the exposure of 700 ML). The right-hand side panels of Fig. 1(a) show the ΔCPD profile vs time after the leak-valve closure [t = 0; a typical pressure-drop profile is shown by the black dashed-dotted line in the middle right-hand side panel of Fig. 1(a)]. Although initiated by the pressure-drop, the relaxation of the ΔCPD is significantly slower. In addition, it is T_{gr}-dependent above the threshold of 70 K, and its rate increases with T_{gr}. This relaxation is presumably the result of a "healing" process the films undergo. Structural defects such as Bjerrum and other protonic defects become mobile at higher growth temperatures, a mobility that also enables the formation of clathrate hydrates.[38,39] For example, Ghosh *et al.*[40–42] demonstrated the formation of hydrates of methane, carbon dioxide, and tetrahydrofuran guests even under UHV and cryogenic conditions. The Bjerrum defects (L/D) enable the reorientation of water molecules, provided that a sufficient thermal activation is available. The possibility to reorient the water molecules allows the transport of excess protons and charged defects for extended distances. Lee *et al.*[43–45] showed that below 130 K, the proton transport through tunneling alone (hopping relay) is the dominant proton transport mechanism, and thus, the transport distance is limited. In the bulk, water molecules are compelled to obey the four-coordinate Bernal–Fowler ice rules.[46] This requirement forms a thermodynamic repulsive force that pushes the protons toward the ASW/vacuum interface where they are stabilized in a three-coordinated planar structure.[43] Thus, at higher growth temperatures, an increased transport of charged defects from the interior toward the ASW/vacuum interface is expected. Furthermore, the propensity of the molecules to rotate faster at the higher temperatures allows the dipoles to be more labile and to reorient according to the local field direction. These self-limiting processes act in the direction of free energy minimization of the system, since they reduce the internal field, which leads to a lower fraction of molecular dipole alignment and thus to lower overall polarization values. These must also contribute to the varied ΔCPD growth profiles observed above 70 K and particularly above 100 K. At the lower growth temperatures, when the available thermal energy is insufficient to initiate this healing process, the polarization of the ASW films is stable for longer periods of time.

When the vacuum recovers, the substrate was cooled down to 33 K [cooling starts at t ≈ 700 s; an example for the cooling profile is shown in the middle right-hand side panel of Fig. 1(a), red dashed line]. For the extra-thick films, the cooling could not reach this base temperature but to ~38 K. During the cooling process, the voltage increases by ~100 mV. Previous studies claimed that ASW films demonstrate pyro- and ferroelectric behavior (manifested by ΔCPD change in response to temperature modifications),[7,10,47,48] since heating–cooling cycles regenerated the voltage across the film.[7] This can explain the small ΔCPD change upon cooling; however, it cannot be responsible for the evolution of the significant polarization we demonstrate here, leaving morphology considerations as the main reason for the observed behavior of the measured polarization as a function of growth temperature (see further discussion in Sec. III C).

B. Internal electric fields

The internal electric field within a film can be obtained from the data presented in Fig. 1 according to Eq. (2). Yet, in order to extract the field, one must accurately translate the film thickness in monolayers to the actual film thickness in length scales. In order to perform such a conversion, one must take into account the porous nature of the ASW films below 115 K.[21] We need, therefore, to know the compact film density, ρ_c, the porous film density (ρ, or equivalently the porosity), which is T_{gr}-dependent, and to consider the interlayer spacing, s (the thickness of a monolayer), which is reported to be 3.7 Å for both amorphous and crystalline water.[49,50] The film thickness can then be calculated as follows: in our experiments, we have adsorbed equal number of molecules for each ASW film (assuming unity sticking coefficient for all temperatures), equivalent to the compact film thickness of 700 ML. Thus, the mass of all the films is equal to that of the compact film. With some simple algebra (see Sec. II of the supplementary material), one obtains the following equation:

$$L = L_c\rho_c/\rho = (\#ML)s\rho_c/\rho, \tag{4}$$

where L is the actual film thickness in length scales and L_c is the compact film thickness. Because we obtain the field from the

constant slope of the ΔCPD profile during growth (above 45 ML), one must define the value of dz,

$$dz \approx \Delta L = \Delta(\#ML)s\rho_c/\rho. \quad (5)$$

Thus, the field can be calculated based on Eq. (2) as follows:

$$E_z = \frac{d(\Delta\mathrm{CPD})}{dz} \cong \frac{\Delta(\Delta CPD)}{\Delta(\#ML)s\rho_c/\rho}. \quad (6)$$

The density values were taken from the work of Berland *et al.*[21] (see also Table SII of the supplementary material; $\rho_c = 0.93$ g/cm^3). We then can calculate the temperature-dependent internal electric field in the growth temperature range of 33 K–100 K. The internal field values derived via Eq. (6) are shown in Fig. 2. These calculations reveal internal electric fields in the range of 10^6 V/m. Once the electric field is known, it allows us to calculate $\tilde{\mu}_z$ according to Eq. (3). Here, we use the van der Waals (vdW) molecular volume, estimated to be 17.35 Å^3.[51] This yields $\tilde{\mu}_z$ in the range of 0.5×10^{-4} D–2.5×10^{-4} D. To calculate the average level of dipole alignment, $\tilde{\mu}_{z(T)}/\tilde{\mu} = \langle\cos\theta\rangle$, where θ is the angle between the water molecular dipole moment and the substrate normal, one needs to know the absolute magnitude of the dipole moment, not only its z-component. This value for either ASW or ice I_h water molecules has not yet been determined experimentally but only for liquid water at 298 K,[52] which is 2.9 D. Dipole moment values calculated from the models based on that of Topping[53] consider only electrostatic interactions among the dipoles themselves and neglect other forces, e.g., hydrogen-bonding or the electrostatic interaction with the metal substrate.[54] An expected value for water dipole moment according to such a model will be ~1.4 D. The smaller value of the dipole moment of the adsorbates relative to their gas-phase value is inherent within these models. Maschhoff and Cowin offered an improved model,[55] the one that does consider the image potential that forms upon adsorption of dipoles on metal substrates and which allows the dipole moment to become higher than its gas-phase value. This model, thus, represents the diploe moment evolution upon the growth of the first monolayers of polar adsorbates, successfully demonstrated for methyl chloride, for example.[31] This model, nevertheless, still lacks a proper representation of the intermolecular forces in water. In contrast, *ab initio* calculations estimate the dipole moment of ice I_h to be in the range of 2.5 D–3.5 D,[56–58] significantly higher than the 1.85 D of the isolated gas-phase water molecule and higher than 2.2 D at the limit of low coverages.[11] The enhancement of the dipole is the result of the attractive potential of molecules due to hydrogen bonding and long-range vdW dispersion forces, affecting intramolecular bond lengths and angles. Therefore, we adopt a value of 3.0 D for the dipole moment of the water molecules in our ASW films. In fact, the dipole moment is expected to increase with the water matrix degree of order because of the increased averaged coordination. Therefore, the expected value for the molecular dipole moment in ice I_h is higher than that of the liquid. Due to the reduced order in ASW and its "glassy" nature, a dipole moment of 3.0 D is considered, which yields an average alignment percentage (normal to the substrate plane) in the range of 0.001%–0.008% (see Fig. 2).

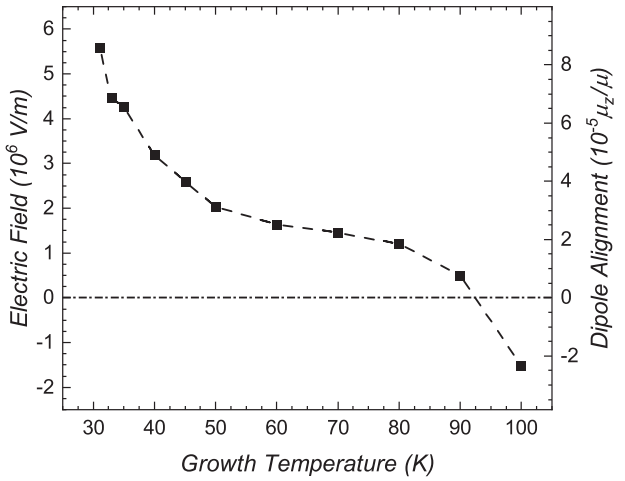

FIG. 2. Internal electric field and the average dipole alignment inside 700 ML-thick ASW films. The average dipole direction flipping is apparent when both the field and the dipole alignment [calculated by Eqs. (6) and (3), respectively] change their sign at T_{gr} between 90 K and 100 K.

The fundamental expression for temperature dependence of the average dipole alignment $\langle\cos\theta\rangle$ with respect to the direction of the electric field is traditionally based on a Langevin function,[9]

$$\langle\cos\theta\rangle = \frac{\mu_{z(T)}}{\mu} = coth\left(\frac{\mu\tilde{E}_z}{kT_{gr}}\right) - \left(\frac{\mu\tilde{E}_z}{kT_{gr}}\right)^{-1}, \quad (7)$$

where $\tilde{E}_Z$ is the effective local electric field that a dipole is exposed to, considering all the interactions with its surrounding molecules and the macroscopic spontaneously formed field, E_z. To reconstruct properly the spontaneous field and to describe the inflection point and eventually the observed polarization flipping ($\mu_z/\mu = 0$), one must well describe the temperature dependence of $\tilde{E}_Z$. In the case of ASW films, this temperature dependence affects more than only the frustrating vdW interactions with the adjacent dipoles, which were suggested by D. Field and co-workers to be the primary feedback mechanism in their "spontelectrics" model.[59] Water molecules form hydrogen bonds, which are significantly stronger than the vdW forces. Moreover, polarization in ASW films is correlated with their porous structures. This forms a complex temperature dependence of $\tilde{E}_Z$. These considerations may also contribute to the spontaneous development of polarization observed for solid films of ammonia and of short alcohols ($C_nH_{2n+1}OH$, n = 1–5).[60,61] Although we do not offer a better representation of the growth temperature dependence of $\tilde{E}_Z$, we still believe that, as will be discussed below, ASW can be qualitatively associated with the family of "*spontelectric*" *materials*, a group of films composed of organic polar molecules that during their growth under similar conditions spontaneously develop an internal electric fields.

C. Thermally activated depolarization

Following their growth and cooling, all the ASW films were annealed by ramping the substrate temperature at a rate of 1 K/s from 33 K to 300 K, beyond the complete desorption of the

first water monolayer from Ru(0001) at ~250 K. Figure 3 depicts the ΔCPD spectra during film heating [TP-ΔCPD measurement; Fig. 3(a)] and their temperature derivative [d(ΔCPD)/dT; Fig. 3(b)]. At temperatures below their corresponding T_{gr}, all the TP-ΔCPD profiles slowly decrease during annealing and the sharply further decrease above their T_{gr}. At ~130 K, the ΔCPD reaches a minimum, which is followed by moderate changes and by a T_{gr}-independent sharp and monotonic rise with two characteristic steps until the film is fully desorbed at ~250 K.

The d(ΔCPD)/dT spectra presented in Fig. 3(b) provide a more coherent differentiation between the various T_{gr}-dependent TP-ΔCPD profiles. The observations of voltage evolution during the growth of thick ASW films and their depolarization upon annealing are not unique and were investigated utilizing TP-ΔCPD measurements by others. These earlier studies demonstrated similar profiles to those shown here.[7,10,11,14,62,63] However, our specific focus on the so-far ignored d(ΔCPD)/dT spectra provides further insights into the existing understanding. The d(ΔCPD)/dT spectra show multiple peaks, among them are the high intensity, T_{gr} dependent minima obtained at low temperatures, which will be discussed in more detail below.

As mentioned previously, TP-ΔCPD measurements and, in particular, their d(ΔCPD)/dT spectra can be compared to standard ΔP-TPD measurements. The d(ΔCPD)/dT produces a desorption-like spectrum, providing information on structural changes the films undergo while annealed, since it is based on the rates of polarization change. However, unlike ΔP-TPD, d(ΔCPD)/dT is sensitive to structural changes significantly below the onset of desorption. The comparison between ΔP-TPD and d(ΔCPD)/dT spectra of several water layers on Ru(0001) show the emergence of three peaks in both measurements: at 160 K, 185 K and at 214 K (at the heating rate of 1 K/s).[11] The 160 K peak is assigned to the desorption of the multilayer, and the two highest temperature peaks are attributed to the desorption of the first monolayer; the 185 K peak is assigned

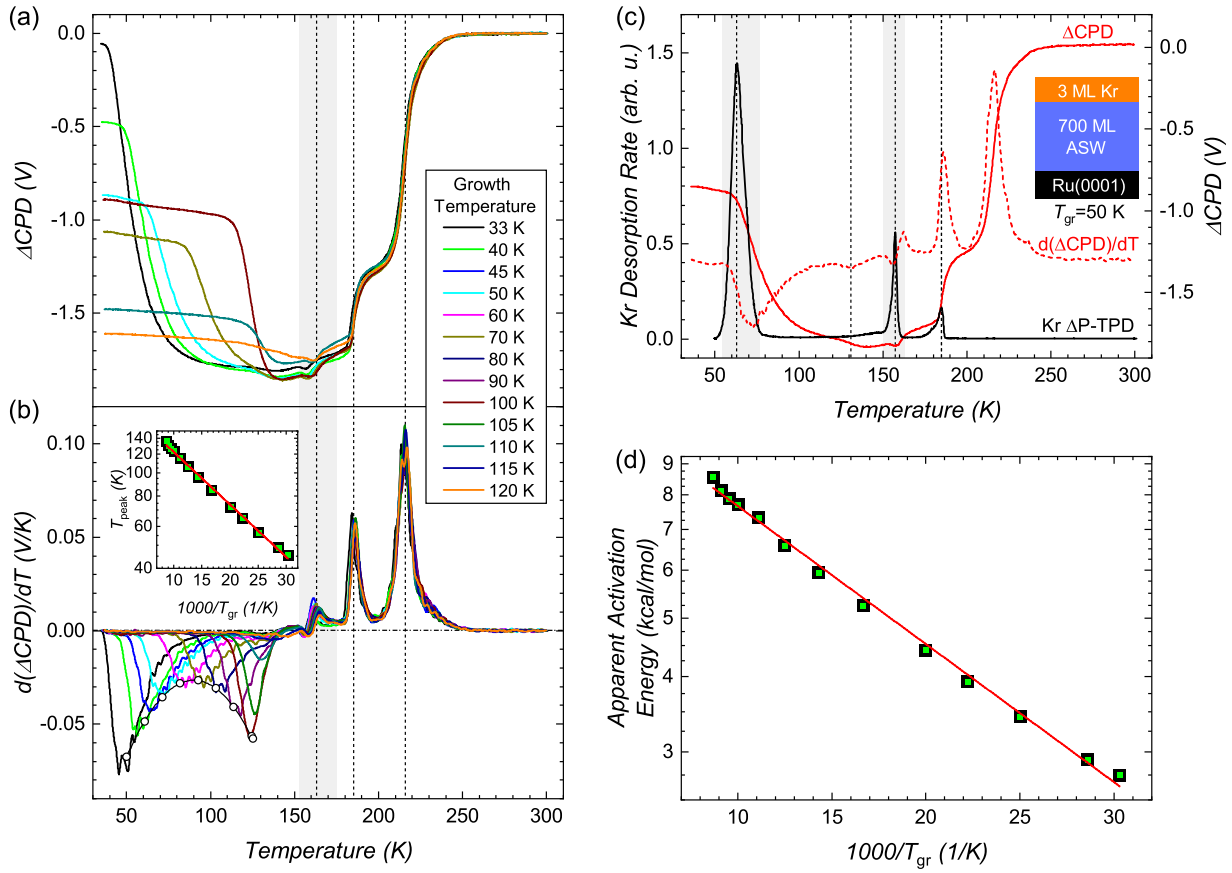

FIG. 3. ASW polarization response to temperature modifications. Temperature-programmed contact potential difference (TP-ΔCPD) measurements (a) and their temperature derivative [d(ΔCPD)/dT; (b)] for 700 ML-thick ASW films grown at T_{gr} in the range of 33 K–120 K that were subsequently cooled down to 33 K prior to their annealing at 1 K/s rate. Connected open circles—a parabolic envelope of the peak intensities. [Inset of (b)] Peak position (T_{peak}; logarithmic scale) plotted vs the inverse of the growth temperature. (c) A comparison between the TP-ΔCPD spectrum (red solid line) and its temperature derivative (red dashed line) of 700 ML-thick films grown at 50 K, and a Kr ΔP-TPD measurement (m/z = 84; solid black line) adsorbed at 50 K on top of an equivalent film (see a schematic in the inset). (d) Apparent activation energy for thermal depolarization of the ASW films, derived by a Redhead-like analysis of the d(ΔCPD)/dT main minimum presented in (b), plotted vs the reciprocal growth temperature (semi-logarithmic scale). In red is a linear best fit.

to water molecules in direct contact with the ruthenium substrate, while the 214 K water ΔP-TPD peak is assigned to the recombined water molecules that were decomposed on the ruthenium surface during heating of the substrate.[11,64]

There is some difficulty to perform high resolution ΔP-TPD measurements of thick water films such as those investigated here, since they may track desorption from other heated surfaces, such as the thin Ta wires spot welded to the substrate (water deposition was performed by backfilling the UHV chamber). Here, we utilize the adsorption of small quantities of weakly interacting species (e.g., Kr) on top of the ASW films to monitor changes occurring within them prior to their desorption.

Figure 3(c) depicts a Kr ΔP-TPD measurement (atomic mass to charge ratio, m/z of 84; solid black line) at a coverage equivalent to 3 ML deposited at 50 K (thus avoiding multilayer growth) on top of the 700 ML-thick ASW film that was also grown at 50 K [identical to the conditions in Figs. 3(a) and 3(b)]. Being inert, Kr atoms are only weakly bound to surfaces. On the other hand, the porous nature of the ASW film allows the caging/trapping of other coadsorbed atoms/molecules.[17,65,66] These coadsorbates are encapsulated inside pockets and are abruptly released during structural rearrangements the film undergoes, during crystallization or during the multilayer desorption, which occur at high temperatures relative to those needed for Kr to desorb from the clean metal surface (at 58 K).[25] The former events are obviously not associated with desorption of water molecules. Thus, Kr ΔP-TPD measurements in this setup provide a tool for monitoring events occurring at the entire temperature range up to the multilayer water desorption, including temperatures below the onset for water crystallization and desorption (<140 K). These events are also expected to be accompanied by polarization modifications and therefore should also be sensed by ΔCPD measurements, allowing the comparison between the two methods (ΔP-TPD and TP-ΔCPD).

The Kr ΔP-TPD measurement reveals three desorption peaks at 63 K (highest intensity), at 157 K, and at 185 K. The 214 K peak seen in the d(ΔCPD)/dT spectra [red dashed line in Fig. 3(c)] and in low-coverage water ΔP-TPD[11,12] is absent from the Kr ΔP-TPD spectrum as expected. The question is what the origin of the Kr desorption at 185 K might be. Since it cannot be part of water monolayer desorption, the only explanation is that the 700 ML water desorption, as a typical zero-order kinetics, has been shifted from around 160 K–165 K at lower coverages up to 185 K. For sufficiently thick films, this peak gradually overlaps that of the first monolayer (185 K). A direct evidence can be found in Fig. 5 (further discussed below), where the d(ΔCPD)/dT peak gradually shifts from 157 K for a 10 ML-thick film to 206 K for a 22 000 ML-thick film. Hence, the 185 K peak seen in the Kr ΔP-TPD should be attributed to the release of Kr atoms embedded within the water multilayer (700 ML), with a similar explanation for the d(ΔCPD)/dT spectra.

The 157 K desorption peak observed in the Kr ΔP-TPD measurement can be assigned to the crystallization onset of the ASW film, in good agreement with the 156 K crystallization temperature reported by Smith *et al.*[66] It is well accepted that the abrupt release of the caged molecules (the "molecular volcano") occurs during crystallization of the ASW film. This, together with the d(ΔCPD)/dT signal in the 150 K–163 K temperature range, and the observation that the 157 K TP-ΔCPD [solid red line in Fig. 3(c)] peak position and its intensity are growth temperature independent [Fig. 3(b)] and beyond 45 ML also thickness independent [see Figs. 5(b)–5(d) and further discussion], supports our conclusion that this TP-ΔCPD peak correlates with the ASW film crystallization to the thermodynamically favored ice I_h. Figure 3(c) reveals one more (small) feature at 131 K, which appears in all d(ΔCPD)/dT spectra of films grown below 130 K. This may represent the nucleation of the metastable ice I_c, a phase transition the film goes through prior to its crystallization to ice I_h.[49,67] Kr desorption is apparently not sensitive enough to pick-up this phase transition. Finally, the low-temperature Kr desorption peak at 63 K correlates well with the sharp depolarization onset.

So far, we have assigned all the features seen in Figs. 3(a) and 3(b) except for the low-temperature d(ΔCPD)/dT spectral minimum, which monotonically shifts to higher temperatures with T_{gr}. Furthermore, the peak intensity also varies with T_{gr}. In the T_{gr} range of 33 K–70 K, the peak intensity decreases, signifying a gradual decrease in the maximal depolarization rate. This trend reverses for films grown in the temperature range of 70 K–100 K, where the rate of depolarization gradually increases with T_{gr}. Above T_{gr} of 100 K, the low-temperature derivative peak steadily diminishes and cannot be traced anymore in films grown at T_{gr} above 120 K. Interestingly, a correlation between the peak position (T_{peak}) and the growth temperature was found to exponentially extrapolate to T_{peak} = 140 K when plotted against $1/T_{gr}$ [see the inset of Fig. 3(b)]. The peak position, therefore, seems to correlate with the depolarization via an Arrhenius-like kinetics. In Fig. 3(d), a first order kinetics Redhead-like treatment[68] was performed according to the following expression:

$$E_a/RT^2_{peak} = (\nu/\beta)\exp\left[-E_a/RT_{peak}\right], \tag{8}$$

yielding apparent activation energies for depolarization in the range of 2.7 kcal/mol–8.6 kcal/mol for films grown in the temperature range of 33 K–115 K. E_a is the apparent activation energy, R is the gas constant, ν is the pre-exponential factor (held constant at 1×10^{13} s^{-1}), and β is the heating rate (1 K/s).

An interesting observation concerns the symmetry of the low-temperature peak intensities for films grown in the range of 33 K–100 K [connected black open circles in Fig. 3(b)]. The two observations of peak shift and intensity changes seem to originate from the complex ΔCPD profile measured during growth, as demonstrated in Fig. 1(a). The shifted peak with decreasing intensities seen for the growth temperature range of 33 K–70 K follows the internal electric field, which gradually decreases with T_{gr} (Fig. 2), whereas the growing peak intensities at the T_{gr} range of 70 K–100 K reflects the gradually increasing polarization above 10 ML and below the observed break of the ΔCPD vs thickness profile [see the middle-left panel of Fig. 1(a)], which occurs at increasing thicknesses. This thickness range (prior to the profile break) is characterized by the higher internal electric field (larger slope) than that evolves after the break. The diminishing peak intensities obtained for films grown above T_{gr} = 100 K [Fig. 3(b)] can be associated with the decreased density of low-coordinated water molecules in the more compact films, which also affects the turn-over from the −1.75 V ΔCPD minimum [see the bottom-left panel of Fig. 1(a)].

The main explanation for the depolarization observed at low temperatures during the annealing is the shrinkage and collapse of

pores during annealing,[18,69] which decreases the film thickness and increasing the film density. This affects the polarization in several ways. The refractive index of a film (and alternatively its dielectric constant) strongly depends on the density, which are typically extracted through the Clausius–Mossotti and the Lorentz–Lorenz relations.[70] The film effective dielectric constant by itself may be affected by the formation of the larger ASW/vacuum interface. For example, the Maxwell Garnett approximation describes the effective relative dielectric permittivity of a mixture of dielectric media by taking into account their different dielectric constants and their interface geometry.[71] In our case, the porous ASW film has an anisotropic pore shape, which cannot be directly characterized, with a net orientation normal to the substrate. The effective dielectric permittivity is a geometry-dependent tensor and according to this model,

$$\left(\varepsilon_{eff}\right)_{ii} = \varepsilon_{(T)}^{cASW} \frac{\varepsilon_{(T)}^{cASW} + \left[\vartheta_{ii}(1-f)+f\right]\left(1-\varepsilon_{(T)}^{cASW}\right)}{\varepsilon_{(T)}^{cASW} + \vartheta_{ii}(1-f)\left(1-\varepsilon_{(T)}^{cASW}\right)}, \tag{9}$$

where the $\left(\varepsilon_{eff}\right)_{ii}$ is the ii term of the tensor, $\varepsilon_{(T)}^{cASW}$ is the temperature-dependent relative dielectric permittivity of the compact ASW film, ϑ_{ii} is the "geometrical factor" (for example, in the case of pores of cigar-like elongated ellipsoids aligned in the z-axis, $\vartheta_{xx} = \vartheta_{yy} \to 1/2$, $\vartheta_{zz} \to 0$), and f is the volume fraction of the voids ($V_{\text{voids}}/V_{\text{film}}$), i.e., the porosity. If that is the case, the effective dielectric constant is both temperature and morphology dependent. Assuming that the ASW film can be characterized by $\varepsilon_{(T)}^{cASW} = 3.2$ below 150 K and a porosity of 0.3, the z-axis component (normal to the substrate) of the effective dielectric tensor is ~2.5, in reasonable agreement with the value of 2 reported by Tsekouras *et al.*[62]

In a recent publication, we have shown that electron-charged water films, grown at T_{gr} in the range of 50 K–120 K and bombarded by 5 eV electrons at 50 K, undergo a discharge phenomenon at similar temperatures to the depolarization process depicted in Fig. 3.[13] A similar Redhead-like analysis showed thermal binding energies in the range of 4 kcal/mol to 8 kcal/mol, similar to those derived here as a result of depolarization, for the corresponding growth temperatures. We have assigned the low-temperature minimum observed in the d(ΔCPD)/dT measurements to morphology modifications the films undergo upon annealing and demonstrated that water films retain a "memory" of their thermal history. This "memory" effect was also evident in the work of Wang *et al.*[7] These authors compared dielectric measurements conducted on compact crystalline D_2O films grown at 150 K with the TP-ΔCPD profiles of equivalent films charged by hydronium ions, claiming that the abrupt discharge upon heating is accompanied by a sharp jump of the dielectric constant from ~3 below 150 K to more than 150 above 150 K (much higher value than that of liquid water at room temperature). There, the discharge and the dielectric constant abrupt rise occurred around the growth temperature of 150 K. Apparently, the morphology modifications that occur during annealing are responsible for the significant dielectric change. Thus, it would be interesting to see whether there is any correlation between these events (dielectric constant change, discharge, and depolarization of the neutral film) over a wide range of growth temperatures (morphologies). The clear dependence of the trapped-electron discharge on T_{gr} indicates that these phenomena are likely to originate from the same physical process.

It has further been shown by Bu *et al.*[14] that the polarization-drop upon annealing is well-correlated with the diminishing integrated intensity of the absorption peaks near 3700 cm^{-1} associated with the undercoordinated water molecules, measured *in situ* during annealing. The integrated intensity of the 3720 cm^{-1} absorption peak, which is assigned to the two-coordinated water molecule O–H dangling bond and the depolarization observed in the TP-ΔCPD profile nicely overlap. At the same time, the profile of the three-coordinated water molecules that absorb at 3696 cm^{-1} follows only the general trend (of decreasing intensities; perhaps due to the competing transformation of two-coordinated water molecules to three-coordinated on the way to become four-coordinated at the crystalline phase). At low T_{gr}, the porosity governs the water-film voltage buildup by the tilting of dipoles residing on the pore walls, apparently due to their interaction with the top surface dipoles (assuming columnar pores, see the discussion in Ref. 14). When T_{gr} increases, the porosity decreases; thus, the dipoles are less well-oriented and more random, leading to a lower degree of polarization. Our observations support the hypothesis of diminishing surface area, i.e., gradual pore shrinkage and collapse, which occurs in response to film heating. The association of the low-temperature peak observed in the Kr ΔP-TPD with the onset of depolarization, together with the results of Bu *et al.*,[14] indicates that a significant rearrangement process takes place already at these low temperatures.

The results demonstrated here are very similar to those obtained with other polar organic films, members of the newly defined class of spontelectric molecular films.[59] Through a molecular dipole alignment during the adsorption of the molecules on the surface, a significant potential difference develops between the two interfaces of the film (substrate/film and the film/vacuum). The field evolved (here—calculated from the slope of the ΔCPD vs thickness curves) is T_{gr}-dependent and generally decreases when films are grown at higher temperatures (as demonstrated in Fig. 2). Above a critical T_{gr}, no spontaneous polarization can be detected (here—above 120 K). The polarization of the spontelectric materials irreversibly decreases during annealing (see Fig. 4 and discussion below), and when the annealing temperature exceeds a certain temperature, the polarization vanishes [see Figs. 3(a) and 3(b)]. This critical temperature for depolarization during annealing is lower than the critical growth temperature (above which no polarization is built-up) and originates from a "memory" of a thermal history the spontelectric materials keep, an effect that is not observed in ferroelectric materials, and is manifested here by the shift of the low-temperature minima observed in the d(ΔCPD)/dT spectra [see Fig. 3(b)].

Ferroelectric materials similarly develop a macroscopic, T_{gr}-dependent, spontaneous polarization, which is generated through ordering of the dipoles (order–disorder mechanism) and also possess a critical growth temperature, above which the films are non-polar (paraelectric).[9] Above the same critical temperature (the *Curie temperature*), ferroelectric materials reversibly lose/regain their polarization, namely, heating–cooling cycles regenerate the polarization at all temperatures below the Curie temperature.

In their investigations for characterizing organic polar films as spontelectrics, Field and co-workers reported that they could not identify any spontaneous polarization of water films,[59] in contrast to many observations made by others.[6,7,10,14,47,48] The similarities ASW films share with spontelectric materials, e.g., nitrous oxide

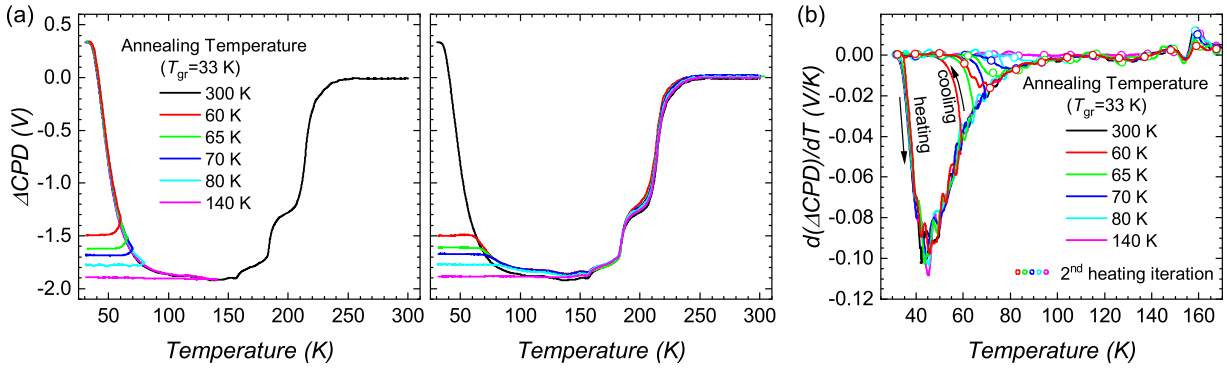

FIG. 4. The irreversible depolarization of ASW films upon annealing. (a) TP-ΔCPD spectra of 700 ML-thick films grown at 33 K, annealed to the indicated temperatures, and cooled back to 33 K (left-hand side panel) and TP-ΔCPD spectra during the second heating iteration of the above films, up to their complete desorption (right-hand side panel). (b) d(ΔCPD)/dT spectra of data shown in (a); the heating–cooling cycle is indicated by the solid lines, whereas the second heating iteration is represented by the connected open circles.

during low-temperature growth, e.g., nitrous oxide, methyl formate, propane, ethyl formate, dihydrofuran, and $CFCl_3$ films,[59] include the general dependence of the electric field and the dipole alignment on the growth temperature. In addition, the recorded nonlinear and multi-trend growth profiles (reported also for methyl formate) and the polarization relaxation after growth termination are similar to the behavior of the spontelectric materials.[59] We can, therefore, conclude this discussion by stating that the ASW films reveal spontelectric-like behavior (including the irreversible depolarization upon annealing, as is discussed next), which originates from their morphology/porosity.

The results presented in Figs. 1 and 3 depict the strong correlation between the growth temperature and the voltage developed between the interfaces, together with a major change of the voltage while heating these films. Data in Fig. 4 reveal that upon heating, the film does not restore the voltage it has gained during growth. This observation rules out the pyroelectric effect from being the physical origin of the spontaneous polarization reported here. 700 ML-thick films were grown at 33 K (thus exhibit the highest degree of porosity/polarization), then annealed to different temperatures (T_{ann}), cooled back to 33 K [Fig. 4(a), left panel], and reheated, this time until the films' complete desorption [Fig. 4(a), right panel; all measurements were conducted with a fresh ASW film]. These TP-ΔCPD profiles are compared with a reference profile of a film that was heated all the way from 33 K to 300 K (i.e., T_{ann} = 300 K; in black). In Fig. 4(b), the d(ΔCPD)/dT spectra of the data shown in Fig. 4(a) are presented (the first heating and cooling cycle in each T_{ann} is indicated by the solid lines and the second heating iteration is in the matching color lines with the open circles). In the first iteration, the annealing follows the reference curve (up to T_{ann}), The second annealing iteration reveals no apparent change in the voltage at temperatures below T_{ann}. Only beyond this threshold, it gradually returns to follow the reference curve.

The d(ΔCPD)/dT profiles [Fig. 4(b)] reveals that both heating cycles (for all T_{ann}) follow the reference curve, however, with hysteresis above T_{ann}. The d(ΔCPD)/dT spectra of the second heating cycle are identical [fixed at d(ΔCPD)/dT = 0] below T_{ann}, which becomes the onset temperature for a gradual return and overlapping the reference spectrum (it takes 10 K–15 K before they overlap again). This hysteresis may arise from the increased time of the film at elevated temperatures during the cooling period, allowing the film to go through further relaxation. The fact that the annealed films eventually coincide with the reference d(ΔCPD)/dT profile means that it does not reproduce the morphology of a film grown at T_{ann}, resulting in some intermediate morphology reflecting the lower level of porosity than that expected at T_{ann}. This is another evidence for the thermal memory effect that was imprinted in the ASW film and leading to the hysteresis shown in Fig. 4.

D. Thickness contribution to film polarization

We have discussed above the contribution of the undercoordinated surface molecules to the film polarization and have shown by Kr desorption that surface reconstruction, caused by the collapse of pores, leads to film depolarization upon annealing. The contribution of the surface sites can further be investigated by varying the film thickness, since the integrated surface area linearly depends on the thickness in the case of fixed porosity (and therefore also the voltage[14]). Furthermore, during desorption of the multilayer, the films demonstrate a T_{gr}-independent dielectric response (manifested by voltage increase), apparent from the overlapping TP-ΔCPD profiles. Thickness-dependent investigation can provide information on the possible rearrangement of the water molecules prior to or during the desorption of the multilayer.

The d(ΔCPD)/dT spectra can differentiate between these two effects and can quantify their contribution to the overall polarization. The first (film reconstruction) will affect the low-temperature peak and hypothetically should follow the kinetics of the reconstruction process, which affects the peak's temperature and expected to linearly increase the peak's area (i.e., the voltage difference). The multilayer desorption peak is expected to shift to a higher temperature with the thickness, since its desorption should follow zero-order kinetics.

In Fig. 5, and Figs. S3 and S4 of the supplementary material, we look deeper into this thickness effect, presenting TP-ΔCPD measurements [see Figs. S3(a)–S3(c) of the supplementary material] and their d(ΔCPD)/dT spectra [see Figs. 5(a)–5(c)] of films in the

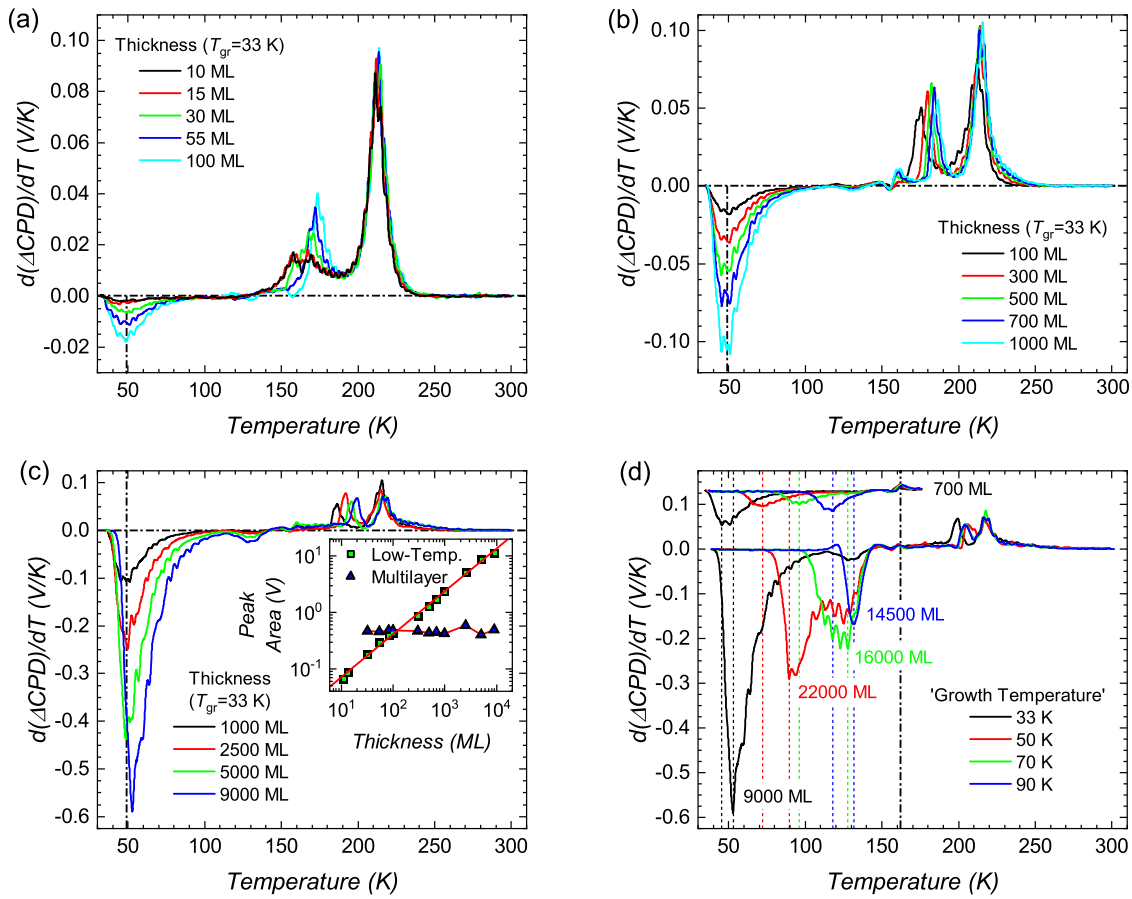

FIG. 5. Film thickness effect on the spontaneous polarization of ASW films. [(a)–(c)] d(ΔCPD)/dT spectra of 10 ML–9000 ML-thick ASW films grown at 33 K. [Inset of (c)] The area under the low-temperature peak (filled squares) and that of the multilayer (filled triangles), calculated from the data in (a)–(c), vs film thickness. The low-temperature peak uptake reveals a power law correlation with the thickness, L (peak area = aL^b, best fit gives b = 0.76). The log–log scale emphasizes the power law correlation, since the exponent is equal to the slope of the linear line. The multilayer uptake does not reveal any distinct thickness dependence. (d) d(ΔCPD)/dT spectra of the "extra-thick" films grown at temperatures in the range of 33 K–90 K.

thickness range of 10 ML to 9000 ML, all grown at 33 K (possessing the highest degree of polarization). The TP-ΔCPD profiles look similar in their general trend to those shown in Fig. 3. All the previously described peaks, except for that of the multilayer desorption, remain at fixed temperatures. The multilayer desorption peak reveals a typical zero-order kinetics, for example, see Fig. S4 of the supplementary material, as was previously discussed; however, its onset shifts with the thickness. In addition, the thickness does not affect the peak area [inset of Fig. 5(c), in filled triangles], and the contribution of the multilayer to the ΔCPD is constant with a value of ~0.5 V. These observations lead to the conclusion that this peak represents the desorption of the ten bottom-most monolayers and that the upper bulk does not contribute to the overall polarization.

The thickness dependence of the low-temperature minimum reveals that the peak temperature does not change, as shown in Figs. 5(a)–5(c), i.e., it behaves similar to a first order kinetics process. The depolarization change (integrated peak area) with the thickness follows a power law, aL^b, where L is the thickness in ML and $b = 0.76 \pm 0.01$ [best fit value; see the inset of Fig. 5(c)]. This deviation from linearity is the result of the ΔCPD-substrate temperature counter-correlation discussed in Sec. III A. The concavity of the ΔCPD as the thickness increases leads to lower levels of polarization than expected, explaining a power correlation smaller than 1.

In Sec. III A, we have discussed the growth of extra-thick films [Fig. 1(b)]. These films were subsequently annealed. Their TP-ΔCPD measurements can be seen in Fig. S3(d) of the supplementary material, whereas the corresponding d(ΔCPD)/dT spectra are demonstrated in Fig. 5(d). The d(ΔCPD)/dT spectra for the extra-thick films, especially those that were grown at elevated temperatures, show a significant shift of the low-temperature peak to higher temperatures as the film thickness increases when compared to that of the thinner films presented in Fig. 3 [and shown again in the inset of Fig. 5(d) for clarity]. This shift is the result of the temperature increase during film growth and can be explained by the "memory" effect of the water thermal history, since

the shift and the temperature increase correlate. In addition, both the low-temperature and the multilayer desorption peaks follow all the trends discussed above—the T_{gr} dependence of the film reconstruction and the thickness dependence of the multilayer desorption. All the other features discussed in this report are not affected. These findings emphasize the effect temperature and thickness have on the spontaneous polarization of ASW films.

IV. CONCLUSIONS

In this work, we have employed continuous contact potential difference (ΔCPD) measurements to investigate the temperature dependence of accumulating spontaneous polarization during the growth of thick amorphous solid water films on a Ru(0001) substrate under UHV conditions. This investigation has been conducted in two domains: the effect of growth temperature and the consequence of film annealing. The ASW film growth responds differently in three temperature regimes, including varying degree of polarization and even a net (average) polarization flipping. The overall measured ΔCPD during growth has contributions from the initial "short range" interaction of the water molecules with the metallic substrate and a "long range" contribution of the net macroscopic dipole alignment. The first is dominated by charge transfer from the adsorbates to the substrate and from the dipole alignment of molecules of the first layers. In addition, this interaction is growth temperature independent and is limited in range, as the ΔCPD signal (-1.7 ± 0.1 V) saturates at the film thickness of 10 ML. At higher coverages, a spontaneous polarization across the film evolves through a net macroscopic dipole alignment. This contribution was found to have a strong growth temperature and film thickness dependence. Spontaneous internal electric fields in the range of 10^6 V/m are formed, even though the net alignment was calculated to be minor (0.001%–0.008%). This polarization cannot be attributed to any pyro- or ferroelectric effects because it irreversibly decreases upon heating, as was demonstrated by TP-ΔCPD measurements. Instead, it is attributed to film morphology, mostly the porosity and the presence of defects. The enhanced propensity of surface molecules to be undercoordinated causes the surface dipole to partially align perpendicular to the substrate, leading to the measurable ΔCPD.

Moreover, we qualitatively associate the spontaneous polarization that amorphous solid water films develop with the family of *spontelectric* materials due to the similar behavior with respect to temperature-dependent polarization accumulation and the irreversible depolarization while being annealed, indicating that the "memory" of its thermal history is an important feature of these materials. Apparent growth temperature dependent activation energies for depolarization were calculated in the range of 2.7 kcal/mol–8.6 kcal/mol. These results indicate that ASW film morphology affects its dielectric constant.

By combining ΔCPD data with the information obtained from the standard ΔP-TPD measurements of a weakly bound probe atom (Kr), we could interpret features in both the TP-ΔCPD profiles and their temperature derivative to structural rearrangements and phase transitions, in this case, to pore collapse at low temperatures and the crystallization to ice I_c and I_h at 131 K and 157 K, respectively.

SUPPLEMENTARY MATERIAL

See the supplementary material for a more comprehensive (quantitative) representation of the ΔCPD measurements during the growth of the extra-thick films seen in Fig. 1, a detailed analysis of the concave ΔCPD profiles during growth, and the subsequent TP-ΔCPD measurements of films of varied thicknesses. In addition, the zero-order multilayer desorption, reflected by the film thickness-multilayer desorption peak correlation, is presented. The supplementary material further presents detailed data and calculations concerning the spontaneous polarization, mostly the observed electric fields and dipole alignment.

ACKNOWLEDGMENTS

Partial support by the Israel Science Foundation (ISF, Grant No. 52/14) and the German-Israeli Foundation (GIF) is acknowledged. The critical technical support provided by Dr. Eduard Mastov, Marcelo Friedman, Shaul Binyamini, and Alexander Lantsman is greatly appreciated.

DATA AVAILABILITY

The data that support the findings of this study are available within the article and its supplementary material.

REFERENCES

[1] A. C. A. Boogert, P. A. Gerakines, and D. C. B. Whittet, "Observations of the icy universe," Annu. Rev. Astron. Astrophys. **53**, 541–581 (2015).
[2] H. Wang, R. C. Bell, M. J. Iedema, A. A. Tsekouras, and J. P. Cowin, "Sticky ice grains aid planet formation: Unusual properties of cryogenic water ice," Astrophys. J. **620**, 1027–1032 (2005).
[3] A. Rosu-Finsen, J. Lasne, A. Cassidy, M. R. S. McCoustra, and D. Field, "Enabling star formation via spontaneous molecular dipole orientation in icy solids," Astrophys. J. **832**, 1 (2016).
[4] C. R. Arumainayagam, R. T. Garrod, M. C. Boyer, A. K. Hay, S. T. Bao, J. S. Campbell, J. Wang, C. M. Nowak, M. R. Arumainayagam, and P. J. Hodge, "Extraterrestrial prebiotic molecules: Photochemistry *vs.* radiation chemistry of interstellar ices," Chem. Soc. Rev. **48**, 2293–2314 (2019).
[5] A. J. Leadbetter, R. C. Ward, J. W. Clark, P. A. Tucker, T. Matsuo, and H. Suga, "The equilibrium low-temperature structure of ice," J. Chem. Phys. **82**, 424–428 (1985).
[6] K. Kutzner, "Spontaneous polarization of condensing carbon monoxide and other gases with an electrical dipole moment," Thin Solid Films **14**, 49–61 (1972).
[7] H. Wang, R. C. Bell, M. J. Iedema, G. K. Schenter, K. Wu, and J. P. Cowin, "Pyroelectricity of water ice," J. Phys. Chem. B **112**, 6379–6389 (2008).
[8] P. V. Hobbs, *Ice Physics* (Clarendon Press, Oxford, UK, 1974).
[9] C. Kittel, *Introduction to Solid State Physics*, 8th ed. (Wiley, New York, 2005).
[10] M. J. Iedema, M. J. Dresser, D. L. Doering, J. B. Rowland, W. P. Hess, A. A. Tsekouras, and J. P. Cowin, "Ferroelectricity in water ice," J. Phys. Chem. B **102**, 9203–9214 (1998).
[11] Y. Lilach, L. Romm, T. Livneh, and M. Asscher, "The first layers of water on Ru(001)," J. Phys. Chem. B **105**, 2736–2742 (2001).
[12] G. Held and D. Menzel, "Isotope effects in structure and kinetics of water adsorbates on Ru(001)," Surf. Sci. **327**, 301–320 (1995).
[13] R. Sagi, M. Akerman, S. Ramakrishnan, and M. Asscher, "Temperature effect on transport, charging, and binding of low-energy electrons interacting with amorphous solid water films," J. Phys. Chem. C **122**, 9985–9996 (2018).

[14]C. Bu, J. Shi, U. Raut, E. H. Mitchell, and R. A. Baragiola, "Effect of microstructure on spontaneous polarization in amorphous solid water films," J. Chem. Phys. **142**, 134702 (2015).
[15]C. Bu, C. A. Dukes, and R. A. Baragiola, "Spontaneous cracking of amorphous solid water films and the dependence on microporous structure," Appl. Phys. Lett. **109**, 201902 (2016).
[16]C. Bu, D. A. Bahr, C. A. Dukes, and R. A. Baragiola, "The effects of cracking on the surface potential of icy grains in saturn's e-ring: Laboratory studies," Astrophys. J. **825**, 106 (2016).
[17]A. Bar-Nun, I. Kleinfeld, and E. Kochavi, "Trapping of gas mixtures by amorphous water ice," Phys. Rev. B **38**, 7749–7754 (1988).
[18]E. Mayer and R. Pletzer, "Astrophysical implications of amorphous ice—A microporous solid," Nature **319**, 298–301 (1986).
[19]G. A. Kimmel, K. P. Stevenson, Z. Dohnálek, R. S. Smith, and B. D. Kay, "Control of amorphous solid water morphology using molecular beams. I. Experimental results," J. Chem. Phys. **114**, 5284–5294 (2001).
[20]D. E. Brown, S. M. George, C. Huang, E. K. L. Wong, K. B. Rider, R. S. Smith, and B. D. Kay, "H_2O condensation coefficient and refractive index for vapor-deposited ice from molecular beam and optical interference measurements," J. Phys. Chem. **100**, 4988–4995 (1996).
[21]B. S. Berland, D. E. Brown, M. A. Tolbert, and S. M. George, "Refractive index and density of vapor-deposited ice," Geophys. Res. Lett. **22**, 3493–3496, https://doi.org/10.1029/95gl03504 (1995).
[22]K. P. Stevenson, G. A. Kimmel, Z. Dohnálek, R. S. Smith, and B. D. Kay, "Controlling the morphology of amorphous solid water," Science **283**, 1505–1507 (1999).
[23]H. A. Engelhardt, P. Feulner, H. Pfnür, and D. Menzel, "An accurate and versatile vibrating capacitor for surface and adsorption studies," J. Phys. E: Sci. Instrum. **10**, 1133 (1977).
[24]C. Benndorf and T. E. Madey, "Adsorption and orientation of NH_3 on Ru(001)," Surf. Sci. **135**, 164–183 (1983).
[25]H. Schlichting and D. Menzel, "Techniques for attainment, control, and calibration of cryogenic temperatures at small single-crystal samples under ultrahigh vacuum," Rev. Sci. Instrum. **64**, 2013–2022 (1993).
[26]D. L. Doering and T. E. Madey, "The adsorption of water on clean and oxygen-dosed Ru(001)," Surf. Sci. **123**, 305–337 (1982).
[27]D. N. Denzler, S. Wagner, M. Wolf, and G. Ertl, "Isotope effects in the thermal desorption of water from Ru(001)," Surf. Sci. **532-535**, 113–119 (2003).
[28]T. Livneh and M. Asscher, "The adsorption and decomposition of C_2H_4 on Ru(001): A combined TPR and work function change study," J. Phys. Chem. B **104**, 3355–3363 (2000).
[29]H. Pfnür and D. Menzel, "The influence of adsorbate interactions on kinetics and equilibrium for CO on Ru(001). I. Adsorption kinetics," J. Chem. Phys. **79**, 2400–2410 (1983).
[30]H. Pfnür, P. Feulner, and D. Menzel, "The influence of adsorbate interactions on kinetics and equilibrium for CO on Ru(001). II. Desorption kinetics and equilibrium," J. Chem. Phys. **79**, 4613–4623 (1983).
[31]T. Livneh, Y. Lilach, and M. Asscher, "Dipole–dipole interactions among CH_3Cl molecules on Ru(001): Correlation between work function change and thermal desorption studies," J. Chem. Phys. **111**, 11138–11146 (1999).
[32]S. Maier, B. A. J. Lechner, G. A. Somorjai, and M. Salmeron, "Growth and structure of the first layers of ice on Ru(0001) and Pt(111)," J. Am. Chem. Soc. **138**, 3145–3151 (2016).
[33]S. Haq and A. Hodgson, "Multilayer growth and wetting of Ru(0001)," J. Phys. Chem. C **111**, 5946–5953 (2007).
[34]V. Buch and J. P. Devlin, "Spectra of dangling OH bonds in amorphous ice: Assignment to 2- and 3-coordinated surface molecules," J. Chem. Phys. **94**, 4091–4092 (1991).
[35]Y. Horowitz and M. Asscher, "Low energy charged particles interacting with amorphous solid water layers," J. Chem. Phys. **136**, 134701 (2012).
[36]J. Klinger, "Influence of a phase transition of ice on the heat and mass balance of comets," Science **209**, 271–272 (1980).
[37]A. Bar-Nun and D. Laufer, "First experimental studies of large samples of gas-laden amorphous "cometary" ices," Icarus **161**, 157–163 (2003).
[38]A. Demurov, R. Radhakrishnan, and B. L. Trout, "Computations of diffusivities in ice and CO_2 clathrate hydrates via molecular dynamics and Monte Carlo simulations," J. Chem. Phys. **116**, 702–709 (2002).
[39]V. Buch, J. P. Devlin, I. A. Monreal, B. Jagoda-Cwiklik, N. Uras-Aytemiz, and L. Cwiklik, "Clathrate hydrates with hydrogen-bonding guests," Phys. Chem. Chem. Phys. **11**, 10245 (2009).
[40]J. Ghosh, R. R. J. Methikkalam, R. G. Bhuin, G. Ragupathy, N. Choudhary, R. Kumar, and T. Pradeep, "Clathrate hydrates in interstellar environment," Proc. Natl. Acad. Sci. U. S. A. **116**, 1526–1531 (2019).
[41]J. Ghosh, R. G. Bhuin, G. Ragupathy, and T. Pradeep, "Spontaneous formation of tetrahydrofuran hydrate in ultrahigh vacuum," J. Phys. Chem. C **123**, 16300–16307 (2019).
[42]J. Ghosh, R. G. Bhuin, G. Vishwakarma, and T. Pradeep, "Formation of cubic ice via clathrate hydrate, prepared in ultrahigh vacuum under cryogenic conditions," J. Phys. Chem. Lett. **11**, 26–32 (2020).
[43]C.-W. Lee, P.-R. Lee, and H. Kang, "Protons at ice surfaces," Angew. Chem., Int. Ed. **45**, 5529–5533 (2006).
[44]C.-W. Lee, P.-R. Lee, Y.-K. Kim, and H. Kang, "Mechanistic study of proton transfer and H/D exchange in ice films at low temperatures (100–140K)," J. Chem. Phys. **127**, 084701 (2007).
[45]E.-S. Moon, C.-W. Lee, and H. Kang, "Proton mobility in thin ice films: A revisit," Phys. Chem. Chem. Phys. **10**, 4814–4816 (2008).
[46]J. D. Bernal and R. H. Fowler, "A theory of water and ionic solution, with particular reference to hydrogen and hydroxyl ions," J. Chem. Phys. **1**, 515–548 (1933).
[47]X. Su, L. Lianos, Y. R. Shen, and G. A. Somorjai, "Surface-induced ferroelectric ice on Pt(111)," Phys. Rev. Lett. **80**, 1533–1536 (1998).
[48]T. Sugimoto, N. Aiga, Y. Otsuki, K. Watanabe, and Y. Matsumoto, "Emergent high-T_c ferroelectric ordering of strongly correlated and frustrated protons in a heteroepitaxial ice film," Nat. Phys. **12**, 1063–1068 (2016).
[49]L. G. Dowell and A. P. Rinfret, "Low-temperature forms of ice as studied by X-ray diffraction," Nature **188**, 1144–1148 (1960).
[50]K. Thürmer and N. C. Bartelt, "Growth of multilayer ice films and the formation of cubic ice imaged with STM," Phys. Rev. B **77**, 195425 (2008).
[51]Y. H. Zhao, M. H. Abraham, and A. M. Zissimos, "Fast calculation of van der Waals volume as a sum of atomic and bond contributions and its application to drug compounds," J. Org. Chem. **68**, 7368–7373 (2003).
[52]Y. S. Badyal, M.-L. Saboungi, D. L. Price, S. D. Shastri, D. R. Haeffner, and A. K. Soper, "Electron distribution in water," J. Chem. Phys. **112**, 9206–9208 (2000).
[53]J. Topping, "On the mutual potential energy of a plane network of doublets," Proc. R. Soc. London, Ser. A **114**, 67–72 (1927).
[54]A. Natan, L. Kronik, H. Haick, and R. T. Tung, "Electrostatic properties of ideal and non-ideal polar organic monolayers: Implications for electronic devices," Adv. Mater. **19**, 4103–4117 (2007).
[55]B. L. Maschhoff and J. P. Cowin, "Corrected electrostatic model for dipoles adsorbed on a metal surface," J. Chem. Phys. **101**, 8138–8151 (1994).
[56]D. D. Kemp and M. S. Gordon, "An interpretation of the enhancement of the water dipole moment due to the presence of other water molecules," J. Phys. Chem. A **112**, 4885–4894 (2008).
[57]P. A. F. P. Moreira and M. de Koning, "Nuclear quantum fluctuations in ice I_h," Phys. Chem. Chem. Phys. **17**, 24716–24721 (2015).
[58]M. Chen, H.-Y. Ko, R. C. Remsing, M. F. Calegari Andrade, B. Santra, Z. Sun, A. Selloni, R. Car, M. L. Klein, J. P. Perdew, and X. Wu, "*Ab initio* theory and modeling of water," Proc. Natl. Acad. Sci. U. S. A. **114**, 10846–10851 (2017).
[59]D. Field, O. Plekan, A. Cassidy, R. Balog, N. C. Jones, and J. Dunger, "Spontaneous electric fields in solid films: Spontelectrics," Int. Rev. Phys. Chem. **32**, 345–392 (2013).
[60]R. Sagi, M. Akerman, S. Ramakrishnan, and M. Asscher, "Spontaneous polarization of thick solid ammonia films," J. Chem. Phys. **153**, 124707 (2020).
[61]A. N. Pilidi, I. K. Gavra, and A. A. Tsekouras, "Spontaneous polarization of cryo-deposited films for five normal saturated monohydroxy alcohols, $C_nH_{2n+1}OH$, $n = 1–5$," J. Phys. Chem. B **123**, 8505–8511 (2019).
[62]A. A. Tsekouras, M. J. Iedema, and J. P. Cowin, "Amorphous water-ice relaxations measured with soft-landed ions," Phys. Rev. Lett. **80**, 5798–5801 (1998).

[63]J. P. Cowin, A. A. Tsekouras, M. J. Iedema, K. Wu, and G. B. Ellison, "Immobility of protons in ice from 30 to 190 K," Nature **398**, 405–407 (1999).
[64]S. Maier, I. Stass, J. I. Cerdá, and M. Salmeron, "Unveiling the mechanism of water partial dissociation on Ru(0001)," Phys. Rev. Lett. **112**, 126101 (2014).
[65]T. Livneh, L. Romm, and M. Asscher, "Cage formation of N_2 under H_2O overlayer on Ru(001)," Surf. Sci. **351**, 250–258 (1996).
[66]R. S. Smith, C. Huang, E. K. L. Wong, and B. D. Kay, "The molecular volcano: Abrupt CCl_4 desorption driven by the crystallization of amorphous solid water," Phys. Rev. Lett. **79**, 909–912 (1997).
[67]P. Jenniskens and D. Blake, "Structural transitions in amorphous water ice and astrophysical implications," Science **265**, 753–756 (1994).
[68]P. A. Redhead, "Thermal desorption of gases," Vacuum **12**, 203–211 (1962).
[69]J.-B. Bossa, K. Isokoski, M. S. de Valois, and H. Linnartz, "Thermal collapse of porous interstellar ice," Astron. Astrophys. **545**, A82 (2012).
[70]M. Born and E. Wolf, *Principles of Optics*, 6th ed. (Pergamon Press, Oxford, 1980).
[71]V. A. Markel, "Introduction to the Maxwell Garnett approximation: Tutorial," J. Opt. Soc. Am. A **33**, 1244 (2016).